

# Investigation of Bending Trainings, Transformation Temperatures, and Stability of Two-Way Shape Memory Effect in NiTi-Based Ribbons

*K. Mehrabi, M. Bruncko, and A.C. Kneissl*

*(Submitted March 4, 2012; in revised form August 22, 2012; published online November 8, 2012)*

This paper discusses the application of rapid solidification by the melt-spinning method for the preparation of thin NiTi-based ribbons. Generally, the application of rapid solidification via melt-spinning can change the microstructure, improving the ductility and shape memory characteristics and lead to small-dimensioned samples. Several thousand thermal cycles were performed on the trained ribbons using bending deformation procedure, continuously observing the changes in the shape memory and transformation behaviors. These changes are due to the appearance of an intermediate phase which was stabilized probably by the accumulation of defects introduced by thermomechanical training. The influence of training and thermal cycling on characteristics of ribbons was studied by x-ray diffraction and transmission electron microscopy and differential scanning calorimetry. The results displayed that bending training methods were useful in developing a two-way shape memory effect (TWSME). All samples show a shape memory effect immediately after processing without further heat treatment. The addition of copper in NiTi alloys was effective to narrow the transformation hysteresis. The W addition has improved the stability of the TWSME and mechanical properties. The TWSME of ribbons and its stability are well suited for important applications such as microsensors and microactuators.

**Keywords** bending training, shape memory alloys, melt-spinning, NiTi-based alloys, two-way effect

## 1. Introduction

NiTi shape memory alloys (SMAs) have received considerable research attention and are widely used because they combine special functional properties with high mechanical strength (Ref 1). These characteristics are due to the martensitic transformation and its reversion, which can be activated by thermal or mechanical loads. SMAs show good corrosion resistance, wear resistance, and high specific electric resistance (which is beneficial for direct current heating) and can be exploited many times before functional or structural fatigue limit service life (Ref 2).

The possibility to realize even complicated movements with an element of simple design and compact size makes shape memory actuators, especially, very attractive (Ref 3, 4).

One critical concern in the development of two-way shape memory effect (TWSME) is the stability of the shape memory properties. Obviously, unstable transformation cycles with associated difficulties with respect to accurate predictions of materials behavior and device design in the presence of these

instabilities are not desirable for actuator applications. One of the perspective materials for this purpose is SMA rapid solidified ribbon. Constant strain training, which is used in this study, is advantageous for shape memory elements with more complicated shapes, while constant stress training is limited to linear shape changes.

The near equiatomic NiTi alloys are by far the most widely used shape memory materials, due to their excellent thermo-mechanical properties, large recovery strains and stresses, high corrosion resistance and biocompatibility. The addition of ternary alloying elements such as Cu and W to near equiatomic NiTi alloy may markedly affect shape memory characteristics, mechanical properties, in particular temperature and hysteresis of martensitic transformation. The matrix of NiTi alloys can be strengthened by the addition of tungsten and because of the low solubility of W in NiTi, as little as 2 at.% W (corresponds to 6.6 wt.% W) is enough to obtain W-rich precipitates in the NiTi matrix (Ref 5). Partial substitution of Ni by W has only small influences on the transformation temperatures and transformation hysteresis in contrast to other elements such as Hf, Nb, etc.

There are several advantages of rapid solidification over the slower conventional solidification techniques. These are an ability to form metastable phases, increasing the solubility above the equilibrium solubility, decreasing the segregation of additions and refining the microstructure. It is considered that all these effects have resulted to improve shape memory effects in the rapidly solidified ribbons. Many physical properties of melt-spun ribbons, as well as their microstructures, depend sensitively on the values of the processing parameters, such as the wheel speed, gas pressure, melt temperature, and nozzle-wheel gap, etc. (Ref 6, 7).

For practical applications, stability of TWSME and control of transformation characteristics is quite important. Therefore,

**K. Mehrabi** and **A.C. Kneissl**, Department of Physical Metallurgy and Materials Testing, University of Leoben, Leoben, Austria; and **M. Bruncko**, Department of Physical Metallurgy and Materials Testing, University of Leoben, Leoben, Austria and Faculty of Mechanical Engineering, University of Maribor, Maribor, Slovenia. Contact e-mail: kambiz.mehrabi@unileoben.ac.at.

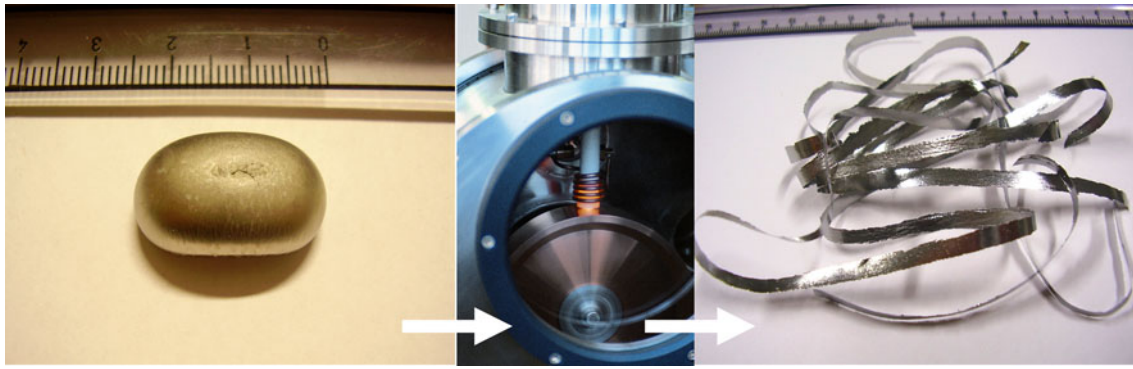


**Fig. 1** Processing steps of transformation from the arc-melted ingots to melt-spun ribbons

**Table 1** Description of the specimens and melt-spinning parameters

No.	Composition	Crucible	Crucible/wheel distance, mm	Nozzle size, mm	Ejection pressure, mbar	Wheel speed, m/s	Melting temperature, °C
1	NiTi	Coated Quartz	0.6, 1, 2, 7, 20	0.9, slit	150	5-30	1350-1400
2	NiTi	Graphite	0.6, 2, 4	1.5	90-200	15-30	1450-1500
3	NiTi2W	Graphite	0.6, 2, 4	1.5	90-200	15-30	1550-1600
4	NiTi25Cu	Coated Quartz	0.6, 2	0.9, 1.5	150	10-50	1300-1350

the main object of this paper was to study the influence of training parameters and thermal cycling on the stability, efficiency, transformation temperatures, and microstructure of melt-spun ribbons.

## 2. Experimental Procedure

The ingots of Ni-50.3at%Ti, Ni-50.3at%Ti-2at%W, and Ni-50.3at%Ti-25at%Cu alloys were prepared by vacuum arc-melting on a water-cooled copper hearth in a reduced Ar atmosphere. To ensure homogeneity, arc-melting was repeated three times for each alloy.

The melt-spun ribbons were produced under a 200 mbar He atmosphere using graphite and quartz-glass crucibles. Ingots (~7 g) were heated to their melting points, determined from phase diagrams, and an additional super heat of 50-250 °C applied to reduce viscosity thereby reducing problems associated with ejection. The molten alloys were ejected using a pure Ar gas overpressure of ~90 to 200 mbar within the crucible onto the cold rotating Cu wheel (200 mm diameter) having a circumferential wheel speed of 5 to 50 m/s to form the ribbon. This resulted in rapid quenching with cooling rates of  $10^3$  to  $10^5$  K/s being achieved. The distances between the nozzle and the wheel surface were 0.6 to 20 mm. Figure 1 shows the transformation of the arc-melted ingots to melt-spun ribbons via the melt spinning processing. It was observed that the quartz crucible reacts with the materials at temperatures above 1400 °C even after coating internally with  $Y_2O_3$ . For high temperature melt-spinning, the best results were achieved using a graphite crucible. Table 1 gives a description of the specimens and melt-spinning parameters.

In this study, different thermomechanical training procedures using bending deformation have been applied on NiTi-based ribbons. One is based on several times thermal cycling

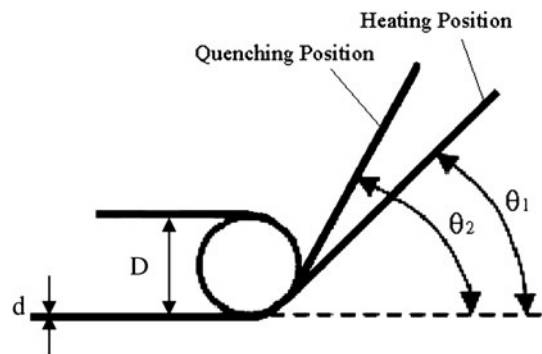


**Fig. 2** Schematic illustration for bending examination of TWSME

under constant bending curvature and then load free thermal cycling and the other one bending below  $M_f$  and load free heating above  $A_f$ .

Tensile specimens with gage size of 20-30 mm in length and 2-4 mm in width were cut from the melt-spun ribbons and tensile tests have performed using a miniature tensile device built by Kamrath & Weiss GmbH. The samples were loaded at a temperature at least below  $A_s$  to detwin the martensite. After unloading, the samples are heated to recover austenite and the original shape. Tensile tests were performed at a constant temperature between 25 and 200 °C, to determine the stress-strain properties of the ribbons.

For TEM studies, thin disks (3 mm in diameter) were mechanically ground to a thickness of 60  $\mu$ m and polished in an electrolyte consisting of 20% sulfuric acid and 80% methanol at 273-278 K by a twin jet electro-polisher (Ref 8). Ion-milling was then performed on the samples for 30 min. The energy of the  $Ar^+$  ions was 3.6 keV, the angle to the surface of the specimen was  $\pm 4^\circ$ , and the specimen was kept at a rotation rate of 3 rpm during ion-milling. Conventional TEM studies were carried out with an acceleration voltage of 120 kV.

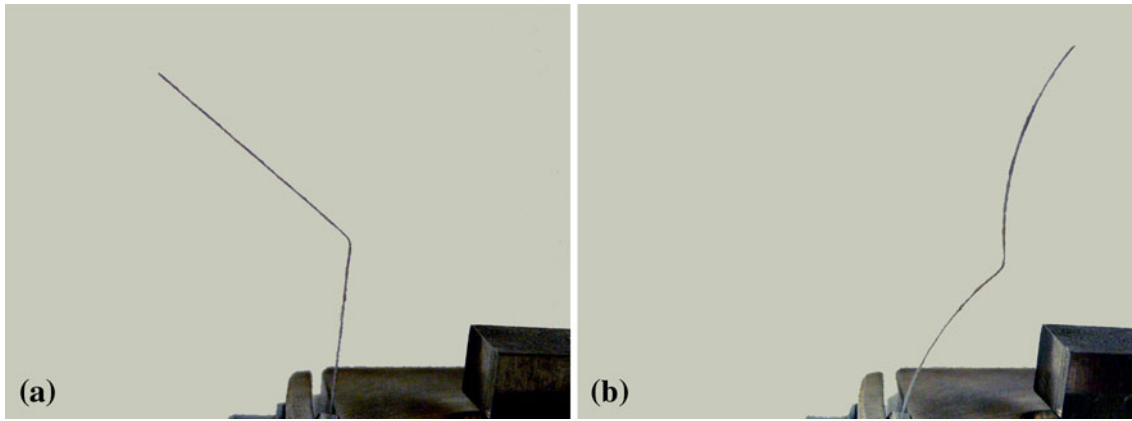


**Fig. 3** Two-way effect of a trained NiTi ribbon: (a) after cooling ( $T < M_f$ ) and (b) after heating ( $T > A_f$ )

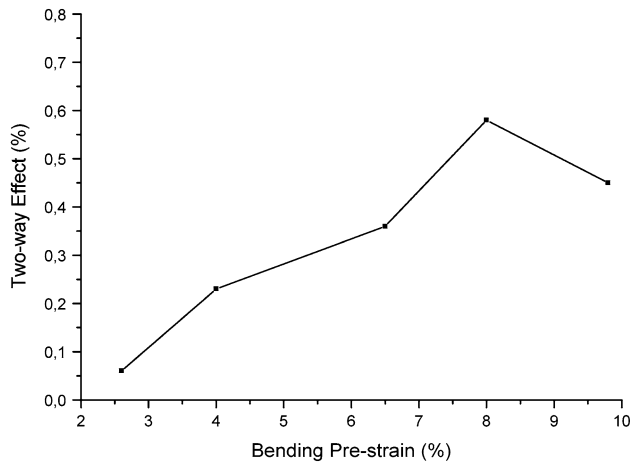


**Fig. 4** Effect of the bending pre-strain on the TWSME of NiTi ribbon

Additionally, the chemical composition of the samples was examined with a TEM, equipped with an EDX analyzer. The crystallographic structure was determined using Bragg-Brentano x-ray diffraction with Cu  $K_\alpha$  radiation at room temperature. The phase transformation temperatures were measured by differential scanning calorimetry (DSC) with different heating/cooling rates. The temperature range of measurements is from  $-40$  to  $180$  °C. A circular sample disk was cut with a punch, put in a  $20\text{-}\mu\text{L}$  pan and closed with a perforated lid.

### 3. Results and Discussion

#### 3.1 Bending Training Procedure

There are several training methods for inducing a two-way shape memory effect, however, two main groups of thermo-mechanical trainings using bending deformation are:

- Thermal cycling with deformation below  $M_f$  (Shape memory cycling)
- Thermal cycling with constant stress or strain (Constrained cycling)

In this section, these two training methods have been applied on NiTi-based ribbons in a self-fabricated device. One is based on bending below  $M_f$  and load free heating above  $A_f$  and the other one based on several times thermal cycling under constant bending curvature and then load free thermal cycling.

The bending deformation strain ( $\epsilon_d$ ) of the outer surface of the specimen was calculated as  $\epsilon_d = d/(D + d)$ , where  $d$  is the ribbon thickness and  $D$  is the diameter of the constrained circle. The one-way shape recovery strain ( $\epsilon_{1w}$ ), two-way shape memory strain ( $\epsilon_{2w}$ ), and plastic deformation ( $\epsilon_p$ ) are measured by the values of:

$$\epsilon_{1w} = [(\theta_0 - \theta_1)/\theta_0] \times \epsilon_d, \quad \epsilon_{2w} = [(\theta_2 - \theta_1)/\theta_0] \times \epsilon_d, \quad \epsilon_p = \theta_1/\theta_0$$

where the angle  $\theta_0 = 180^\circ$  and the deformation angles  $\theta_1$  and  $\theta_2$  are indicated in Fig. 2. The value of spontaneous shape change during heating and cooling was recorded by photographing. During the constrained training and subsequent free thermal cycling, temperature was changed from room temperature (RT) to  $200$  °C. The TWSME was executed several thousand times and the changes in the deformation behavior and the stability of the effect were continuously observed. As example in Fig. 3, a NiTi ribbon is shown that displays reversible shape change during heating and cooling after 500 free thermal cycles.

#### 3.2 TWSME Using Bending Deformation

In this study pieces of NiTi-based ribbons ( $\sim 40$  mm long, 2 mm wide, and  $80$   $\mu\text{m}$  thick) were bent to different small radii from 4 to 0.7 mm. The corresponding bending strains are 2.6, 4, 6.5, 8, and 9.8%. Figure 4 shows the effect of bending strain on the TWSME of NiTi ribbon after 3 training cycles. With increasing strain, TWSME increased to a maximum of 0.58% at 8% strain and then decreased after a deformation to 9.8% due to plastic deformation. Since it was found that 8% bending strain (with bending radius of 0.9 mm) leads to the highest TWSME, the further experiments were performed with that bending strain.

Figure 5 illustrates comparison of TWSME results from both bending training methods. As can be seen, in the first method (shape memory cycling) the TWSME increased with the number of training cycles. It can be seen that after one training cycle only one-way SME exists, while after several cycles a TWSME can be found.

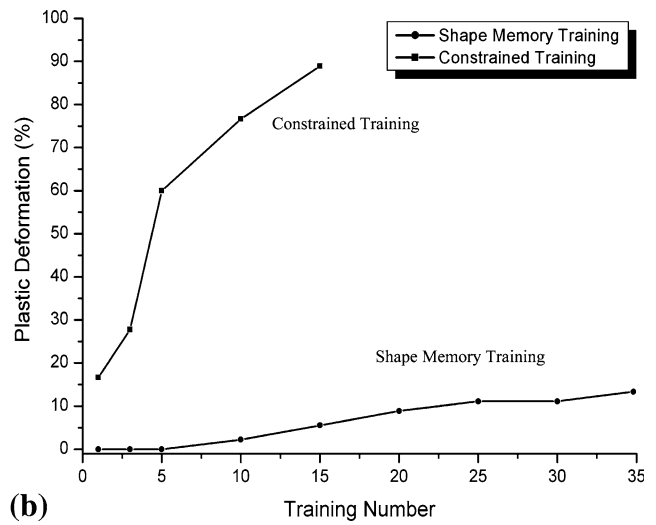
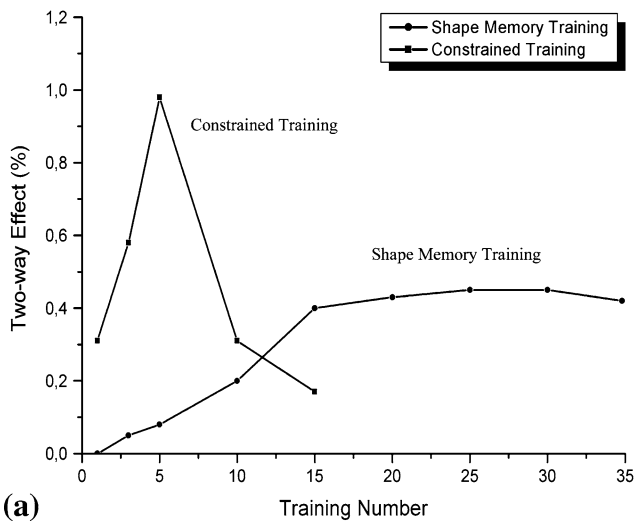


**Fig. 5** Effect of different training methods of NiTi ribbon on: (a) TWSME and (b) plastic deformation

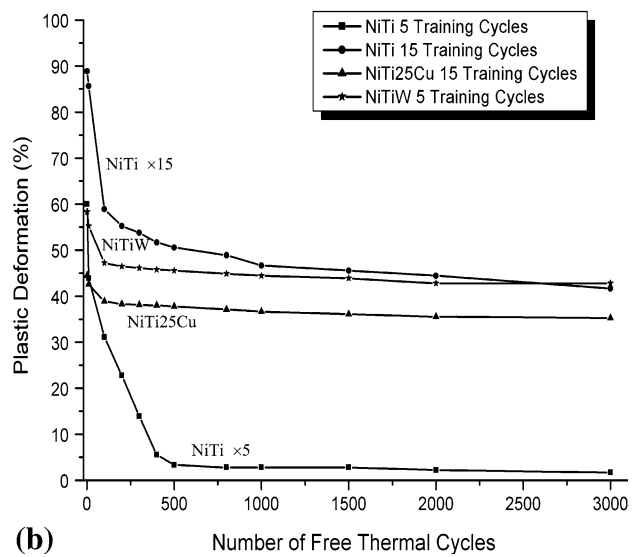
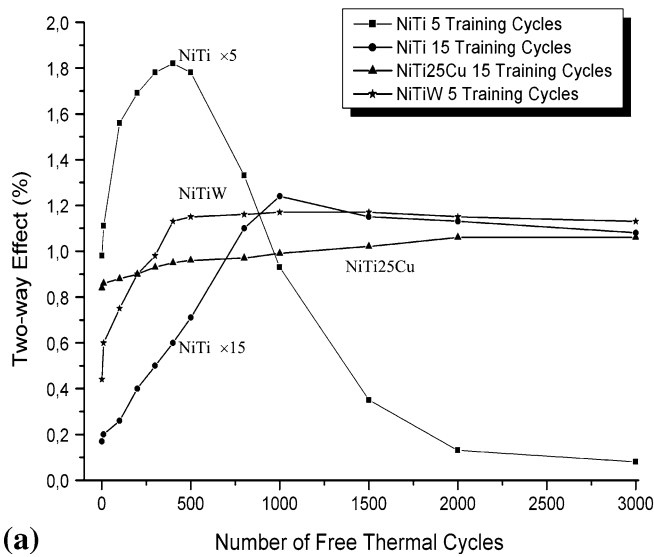


**Fig. 6** Effect of free thermal cycles after constrained training in different NiTi-based ribbons on: (a) TWSME and (b) plastic deformation

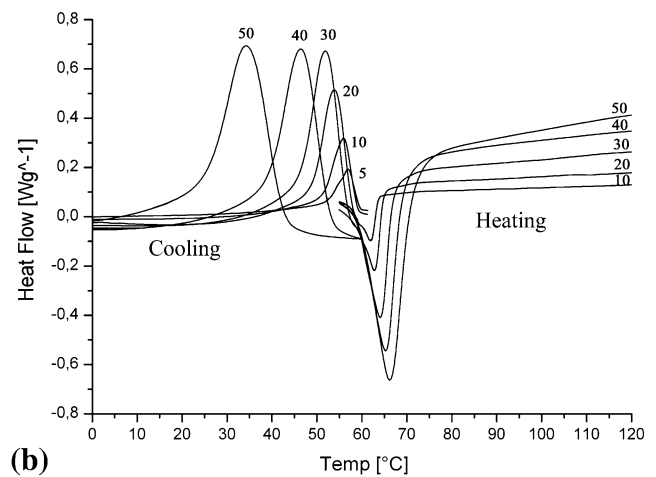
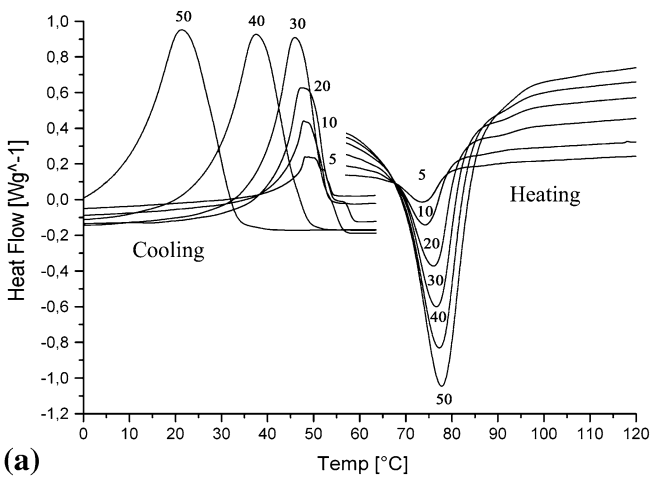


**Fig. 7** Transformation behavior of ribbons at different heating/cooling rates: (a) NiTi and (b) NiTi25Cu

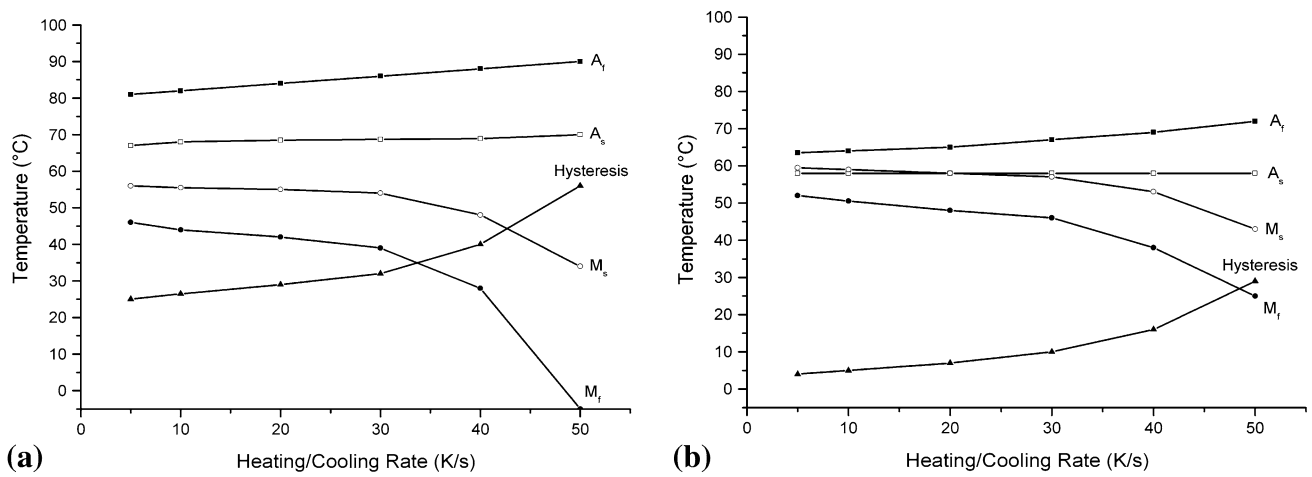


**Fig. 8** Effect of heating and cooling rates on the thermal hysteresis and transformation temperatures: (a) NiTi ribbon, (b) NiTi25Cu ribbon

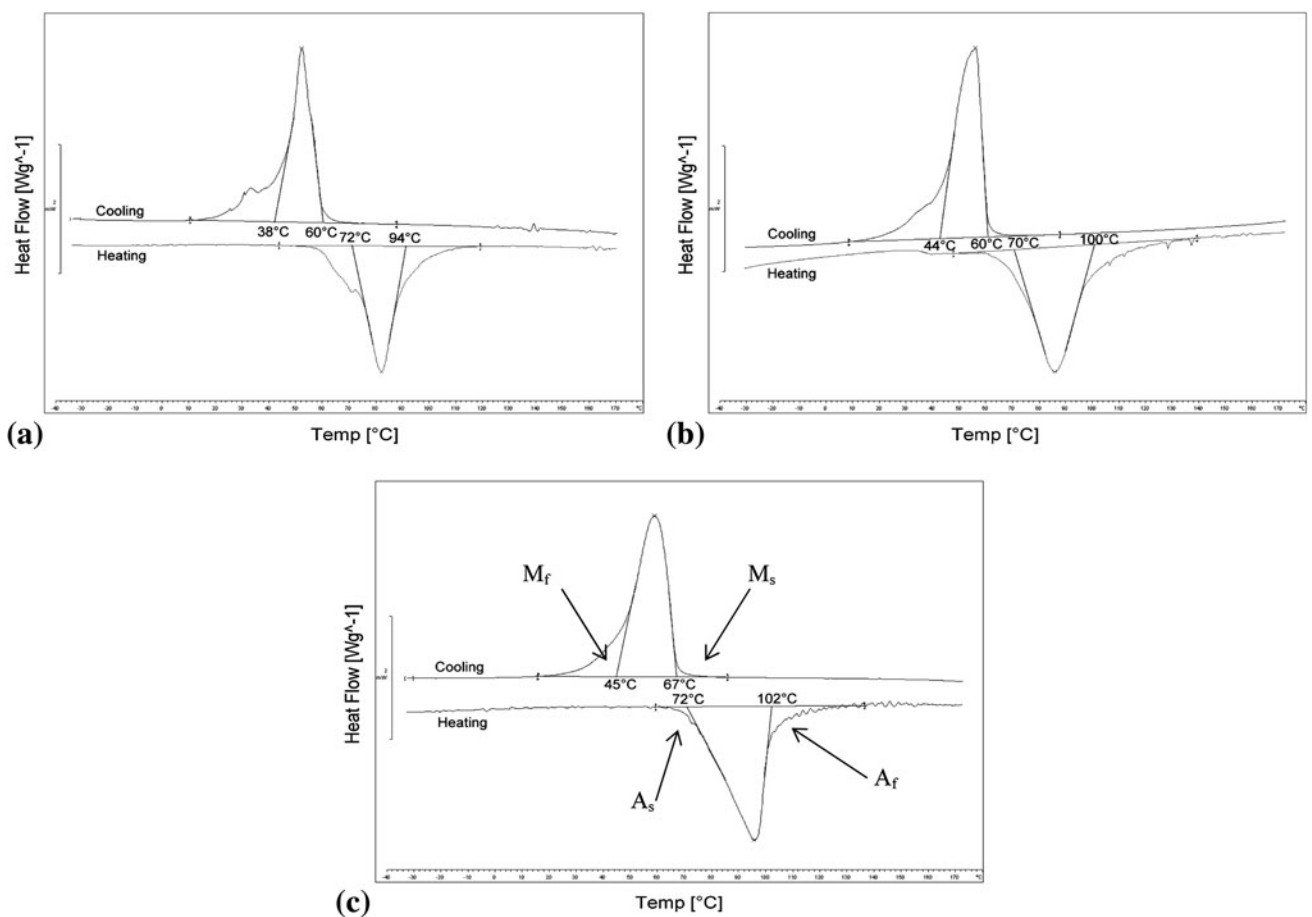


**Fig. 9** DSC curves of NiTi ribbons at various wheel speeds: (a) 5 m/s, (b) 15 m/s, (c) 30 m/s

As shown in Fig. 5(a) at constrained training, the TWSME increases during the first few training cycles much higher than during shape memory training method but afterwards decreases because the plastic deformation increases strongly. The largest TWSME is achieved after 5 constrained training cycles. The experimental results make it clear that during training, the strain energy of bending strain will provide driving force for the

preferential orientation of martensite variants. But with the increase of training cycles, plastic deformation accumulates in the crystal grains with the result of unrecoverable strain. Therefore, one-way and two-way shape memory effect of ribbons will decrease with the increase of training number. In other words, this fact suggests that an appropriate density of slip defects is effective for the improvement of the TWSME

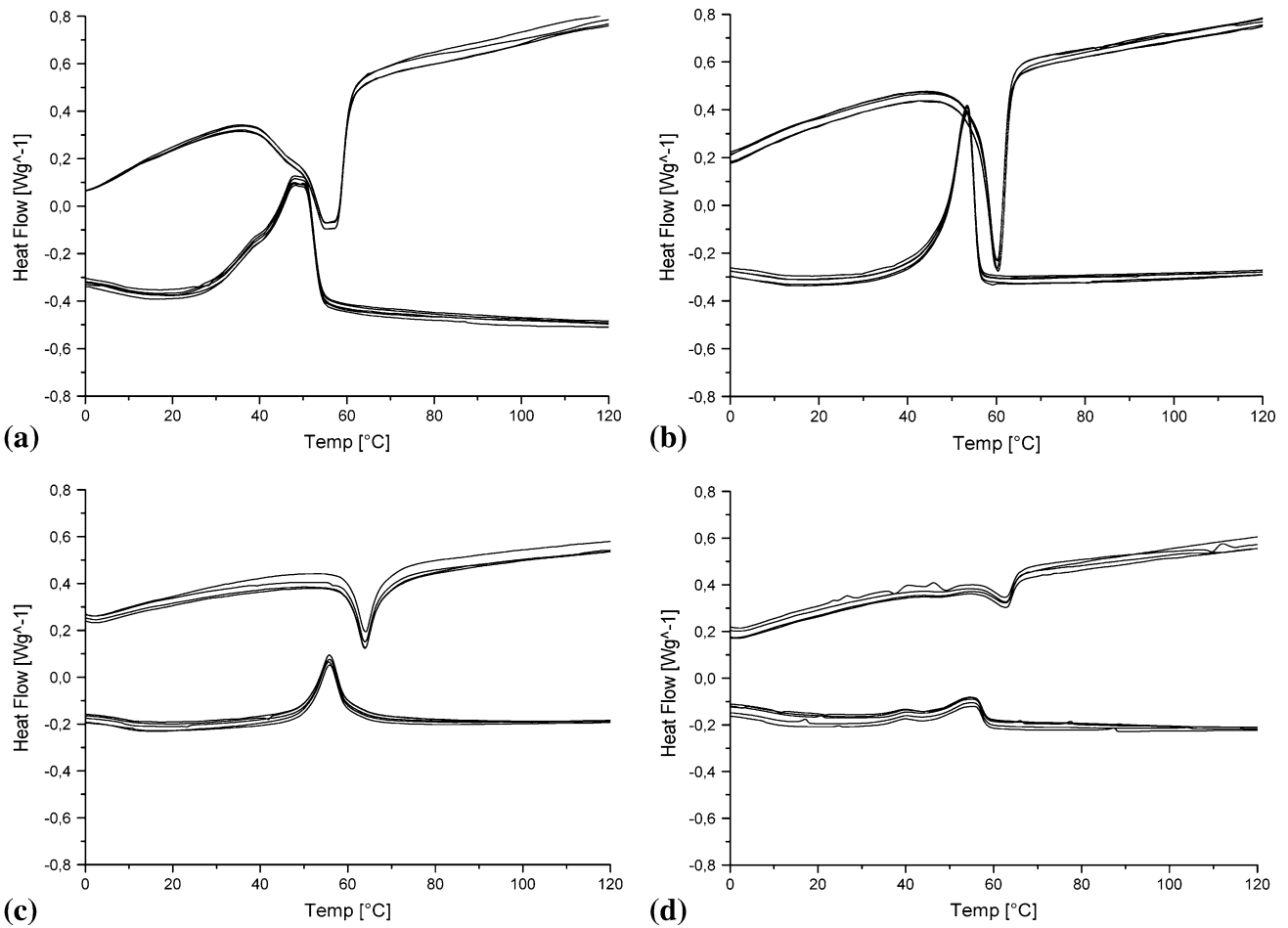


**Fig. 10** DSC curves of NiTi<sub>25</sub>Cu ribbons at wheel speeds of: (a) 10 m/s, (b) 20 m/s, (c) 30 m/s, and (d) 40 m/s

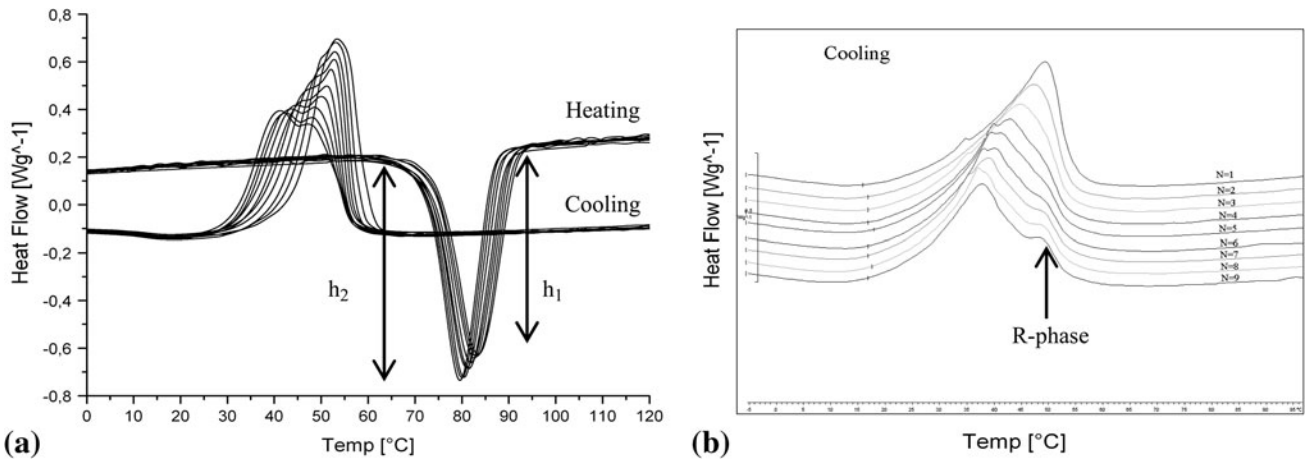


**Fig. 11** DSC results for NiTi ribbons with different numbers of free thermal cycles after one constrained cycle: (a) several thermal cycles and (b) exothermic behavior

while an excessive density of defects and plastic deformation reduce the TWSME.

Eventually, it was found that the constrained training is a more operative method in comparison with shape memory training; therefore, all following trainings in this study were trained by the constrained training method.

### 3.3 Stability of the TWSME

Figure 6 shows the stability of TWSME obtained by constrained training in NiTi-based ribbons. In most cases, after enough constrained training and then several hundred free thermal cycles, the TWSME became larger with higher shape

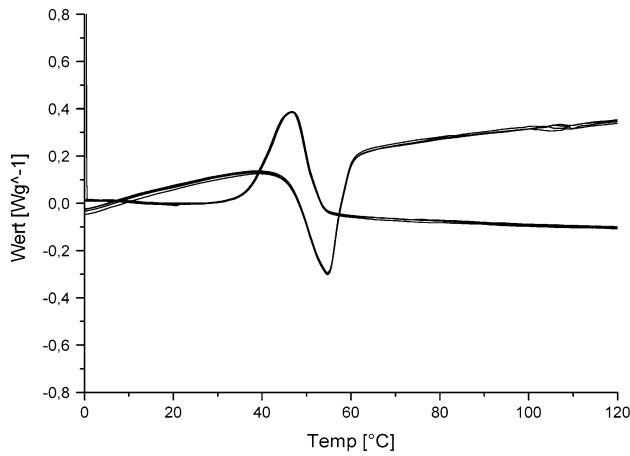


**Fig. 12** DSC for NiTi25Cu ribbons during thermal cycles after training

recovery and finally stabilized. As represented in the Figure, the TWSME of NiTi ribbon trained with 5 constrained cycles was about 1% and after 400 free thermal cycles increased to about 2%, but shows poor stability during the subsequent thermal cycling. When the training procedure is extended to 15 cycles, despite a smaller initial TWSME, the sample shows relatively high stability during 3000 thermal cycles.

Similar to NiTi ribbon, the NiTi25Cu ribbon demonstrated that 5 training cycles were not effective enough to stabilize TWSME and a good stability can be got only after 15 training cycles, however, the NiTi2W ribbon leads to a TWSME with proper stability already after 5 training cycles. This is due to higher strength of NiTi2W ribbon which causes enough internal stress fields already after 5 training cycles. In Fig. 6, the TWSME and plastic deformation of various ribbons were observed during 3000 thermal cycles. Softer ribbons can be trained easily to higher effect size but the stability is weak. On the other hand, ribbons of higher strength exhibit smaller TWSME values but prove to be relatively stable against functional fatigue. The stability of about 1% TWSME in these ribbons seems very suitable for many technical long-term applications.

The decrease of TWSME and plastic deformation in NiTi ribbons after a high number of thermal cycling may be related to partial relaxation of the stress field or rearrangement of dislocations formed by the training process and the redistribution of existing defects (dislocations).

### 3.4 Transformation Behavior Before Training

Figure 7 shows the transformation behavior in the NiTi and NiTi25Cu alloys. To find on the transformation characteristics of rapid solidified ribbons and the most proper heating/cooling rate for investigation of the transition temperatures, the transformations were studied by means of DSC measurements at various cooling/heating rates. These rates were ranging from 50 to 5 °C/min. The results have shown that the heating/cooling rate has strong influence on the transformation temperatures and the absorbed/released heat during transformation.

It is evident that the latent heat of the transformation decreases with decreasing heating/cooling rate. In addition,  $A_s$  and  $A_f$  are fairly stable at various heating/cooling rates, while after a critical rate (30 °C/min),  $M_s$  and  $M_f$  decrease with the increment in heating/cooling rate.

Therefore with increasing heating/cooling rate, thermal hysteresis increases significantly as well. It can be explained that dislocations associated with high heating/cooling rates generate an internal stress state which restricts the transformations (Ref 9).

Figure 8 shows the starting and finishing temperatures of the transformations and the measurement of transformation hysteresis, defined as  $A_f - M_s$ , determined from the DSC curves shown in Fig. 7. As displayed in Fig. 8, thermal hysteresis decreased continuously with decreasing heating/cooling rate. Also as expected, NiTi25Cu ribbons demonstrate much smaller transformation hysteresis than NiTi ribbons. Finally in this work, the heating/cooling rate was taken to be  $\pm 20$  °C/min for all further DSC studies.

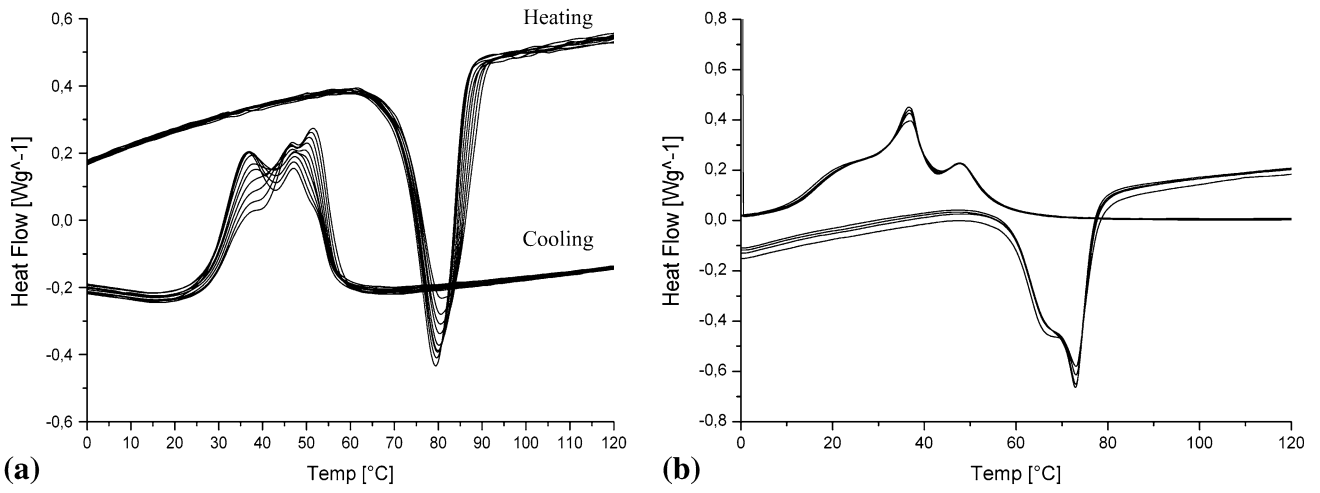
Figure 9 displays DSC curves for the NiTi melt-spun ribbons produced at wheel speeds of 5, 15, and 30 m/s. Figure 9(a) shows the phase transformation for the lowest wheel speed and therefore lowest cooling rate while Fig. 9(b) and (c) represents the higher wheel speeds and cooling rates. There is only slight difference in the transformation temperatures but additional peaks appeared at the lower cooling rates (especially Fig. 9a). These additional peaks are attributed to the fact that the transformation temperatures of the chilled side are different from those of the free side of the ribbons. In addition, the materials exhibit higher segregation at lower cooling rate, causing new peaks in the DSC curve.

Figure 10 shows the transformation of NiTi25Cu ribbons after melt-spinning with various wheel speeds, ranging from 10 to 40 m/s. The transformation becomes more evident and sharper with lower wheel speeds, i.e., lower cooling rate. The high cooling rate causes high amount of defects and internal stress in ribbons and these defects play an important role in the transformation behavior of the phases. The ribbons produced with wheel speeds of 40 m/s have mostly amorphous structures.

### 3.5 Transformation Behavior and Properties After Training

In many applications the shape memory components experience repeated thermal cycles, either under external load or free of constraint. One critical concern in the development of devices using SME is the functional property stability of the alloys. It is known that the critical temperatures and the internal stresses for the martensitic transformation in NiTi-based alloys are sensitively affected by thermal cycling. Therefore, understanding of the effects of training and subsequent thermal cycling on the transformation behavior has been an important concern for the SMAs.

The transformation behavior of a NiTi ribbon with increasing number of free thermal cycles after one constrained training cycle is shown in Fig. 11. The numbers in the figure correspond to the number of free thermal cycles. Thermal cycling decreases slightly the transformation temperatures, especially the critical temperatures for both the forward (martensite) and the reverse (austenite) transformations. Moreover as can be seen in Fig. 11(a), the height of the peak of austenitic phase transformation increases mildly during thermal cycling ( $h_1 < h_2$ ). The decrease in austenitic transformation temperatures (heating) and the increase in the height of the austenitic peak indicate an easier transformation from martensite to austenite which is generally ascribed to the presence of a dislocation structure that serves as a network of nucleation sites for the austenite phase. It is already established (Ref 10-13) that this drop in transformation



**Fig. 13** DSC for NiTi ribbons during thermal cycles after: (a) 500 cycles, (b) 3000 cycles

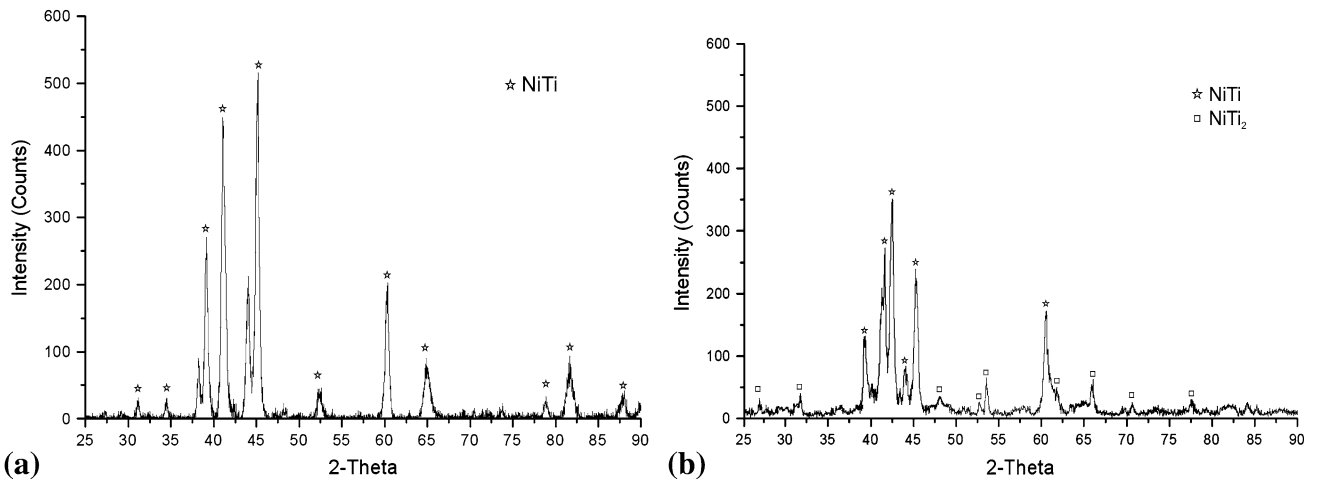


**Fig. 14** XRD pattern of a NiTi ribbon: (a) before training, (b) after constrained and free training cycles



**Fig. 15** TEM micrograph of the B19' martensite microstructure in a melt-spun NiTi ribbon: (a) before training, (b) after training showing Ti<sub>2</sub>Ni particles with related SAD pattern



temperatures during thermal cycling is due to the defect generation and internal stresses induced during fabrication and subsequent thermomechanical treatment.

The exothermic behavior (during cooling, Fig. 11c) of the transformation shows that a broad peak with a shoulder on the right side (arrow) appears during thermal cycles, which is very close to the main peak. This phase is R-phase or pre-martensitic transformation. The austenite to martensite transformation temperature gradually decreases with increasing thermal cycles, while the R-phase transformation remains relatively constant. As has been reported also in (Ref 14-17), the appearance of R-phase is common for plastically deformed or thermally cycled near-equiatomic NiTi alloys, since dislocations or precipitates create energy barriers for martensite nucleation, making the R-phase formation a lower energy alternative. Inducing small areas of R-phase can relax the internal stress associated with the dislocations or precipitates. The R phase is probably present ever since the first cycle. Its apparent development is not due to the thermal cycling but to the fact that  $M_s$  is shifted to lower temperatures during thermal cycles. For the NiTi ribbon, as exhibited in Fig. 11, it is found that the transformation temperatures are not stable in early stages and each cycle of DSC leads to lower transition temperatures ( $\sim 1$  °C/cycle), at least for the first 10 cycles.

For NiTi25Cu alloys as displayed in Fig. 12, DSC curves of the melt-spun ribbon with wheel speed of 20 m/s after 5 constrained training cycles show that the transformations are much more stable than the same ribbon before training (Fig. 10b). The decrease in  $M_s$  temperature due to DSC cycling is less than 0.2 °C/cycle. Also comparison of the NiTi25Cu ribbons before and after training revealed that the transformation peaks of trained ribbon become smaller and wider. This may be explained by the increase of the number of nucleation sites and dislocations.

**Table 2 EDX results from the matrix and NiTi<sub>2</sub> particles**

	Ti, at. %	Ni, at. %
NiTi-matrix	51.1	48.9
NiTi <sub>2</sub> particles	66.5	33.5

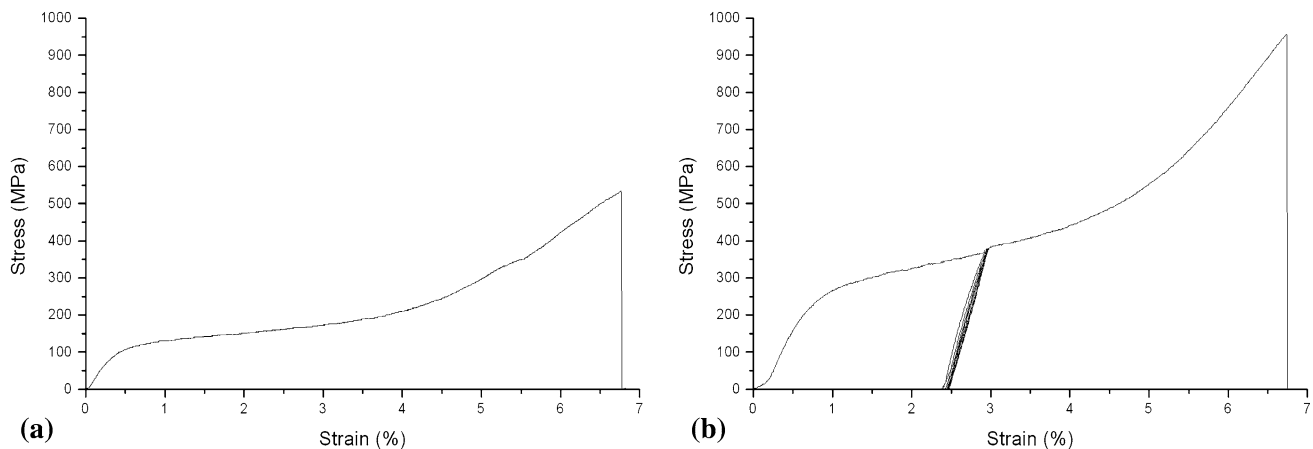


**Fig. 16** Stress–strain curve from the melt-spun ribbon: (a) before training, (b) after training

In addition, DSC curves of trained NiTi ribbon (5 constrained cycles) after 500 and 3000 free training cycles are shown in Fig. 13. After these free trainings, a multiple-stage martensitic transformation by thermal cycling occurred. This is probably associated with R-phase formation and martensitic transformation performed with several steps due to the strain fields around coherent precipitates. Also occasionally some precipitates form and grow during the thermomechanical training, which generates large-scale heterogeneity in microstructure and chemical composition. Therefore some regions undergo a B2-R-B19' two-stage transformation, while the other regions, being free of precipitates, undergo a direct B2-B19' transformation.

Furthermore, as exhibited in Fig. 13(b), after sufficient free thermal cycling, when the defects are stabilized, the amount of the shift lessens and a significant stability in the transformation temperature could be seen. This is attributed to the strengthening of the matrix and introduction of precipitates in the matrix.

Results from XRD pattern from the melt-spun ribbons before and after thermomechanical training indicate that the formed precipitates are Ti<sub>2</sub>Ni (Fig. 14). All peaks in the pattern before training belong to the B19' martensite, while after 5 constrained cycles and 500 free training cycles Ti<sub>2</sub>Ni precipitates are present. It is thought that many nanosize Ti<sub>2</sub>Ni precipitates have been grown during training and thermal cycles.

Furthermore, TEM was employed to investigate the substructures of NiTi ribbons before and after training procedure. Figure 15 displays a fine martensitic structure (B19' phase) with nano-sized twin boundaries. The corresponding TEM micrograph after 5 constrained cycles and 500 free thermal cycles shows that many fine spherical particles were precipitated inside the martensite grains. By selected area diffraction and by EDX analysis (Table 2) these particles (indicated by arrows) could be identified as Ti<sub>2</sub>Ni. The size of the precipitates was estimated to be in the order of several hundred nanometers.

To examine the effect of training on the mechanical properties of NiTi ribbons, a tensile test was performed before and after training procedure. The results of the tensile tests are shown in Fig. 16. The increase in strength is caused probably by the Ti<sub>2</sub>Ni precipitates and a higher dislocation density. Moreover, unloading-reloading tests have been performed 5

times for trained ribbon. The deviation between the unloading path and reloading path is very small. This experimental result reveals that the deformation of the specimen is fully pseudo-plastic and that there is no austenite phase and pseudoelastic effect at all.

It is well known that, in NiTi alloys, the appearance of an intermediate phase can take place due to the increasing number of thermomechanical training, thermal cycling, aging at an appropriate temperature and processing techniques (Ref 18). The transformation to an intermediate phase in NiTi brings about good mechanical properties (strength and ductility) and an excellent shape memory property. Therefore, the presence of the intermediate phase is useful in engineering fields (Ref 19).

#### 4. Conclusions

- Thin NiTi-based ribbons were produced by rapid solidification technique and shape memory effects immediately after processing without subsequent heat treatment. TWSME has been successfully introduced by different bending training methods.
- The NiTi and NiTi25Cu ribbons demonstrated that 5 training cycles were not effective enough to stabilize the TWSME, and a good stability can be reached only after 15 training cycles, however the NiTi2 W ribbons achieve a TWSME with proper stability already after 5 training cycles.
- The W and Cu additions have improved the stability of the TWSME. The addition of copper was also effective to narrow the transformation hysteresis, which is very important for applications that require short response time at thermal cycle, such as actuators and sensors.
- After free thermal cycling of trained NiTi, many fine Ti<sub>2</sub>Ni spherical particles were observed by XRD and TEM and therefore, the trained ribbons show higher strength than ribbons without training.

#### References

1. J. Frenzel, Z. Zhang, K. Neuking, and G. Eggeler, High Quality Vacuum Induction Melting of Small Quantities of NiTi Shape Memory Alloys in Graphite Crucibles, *J. Alloys Compd.*, 2004, **385**, p 214–223

2. S. Miyazaki, T.W. Duerig, K.N. Melton, D. Stockel, and C.M. Wayman, Ed., *Engineering Applications of Shape Memory Alloys*, Butterworth-Heinemann Applications, London, 1990, p 394
3. Y. Liu, J. Laeng, T.V. Chin, and T.H. Nam, Effect of Incomplete Thermal Cycling on the Transformation Behaviour of NiTi, *Mater. Sci. Eng., A*, 2006, **435–436**, p 251–257
4. P. Ochin, V. Kolomytsev, A. Pasko, P. Vermaut, F. Prima, and R. Portier, Phase Transformations in Rapidly Solidified (Ti-Zr)<sub>50</sub>(Ni-Cu-Sn)<sub>50</sub> Alloys, *Mater. Sci. Eng., A*, 2006, **438–440**, p 630–633
5. A.C. Kneissl, K. Mehrabi, M. Bruncko, B.J. McKay, and D. Uhlentaut, Characterization and Properties of NiTi(W) and CuAlNi Shape Memory Alloys, *Int. J. Mater. Res. (Z. Metallkd.)*, 2009, **100**, p 1038–1045
6. Y.-W. Kim, Y.-M. Yun, and T.-H. Nam, The Effect of the Melt Spinning Processing Parameters on the Solidification Structures in Ti-30 at.% Ni-20 at.% Cu Shape Memory Alloys, *Mater. Sci. Eng., A*, 2006, **438–440**, p 545–548
7. M.J. Kramer, H. Mecco, K.W. Dennis, E. Vargonova, R.W. McCallum, and R.E. Napolitano, Rapid Solidification and Metallic Glass Formation—Experimental and Theoretical Limits, *J. Non-Cryst. Solids*, 2007, **353**, p 3633–3639
8. L.J. Chiang, C.H. Li, Y.F. Hsu, and W.H. Wang, Effects of Thermal Cycling on Multiple-Stage Transformation in Ti<sub>49.3</sub>Ni<sub>50.7</sub> Shape Memory Alloy, *J. Alloys Compd.*, 2008, **462**, p 47–51
9. K. Nurveren, A. Akdogan, and W.M. Huang, Evolution of Transformation Characteristics with Heating/Cooling Rate in NiTi Shape Memory Alloys, *J. Mater. Process. Technol.*, 2008, **196**, p 129–134
10. K.N. Lin and S.K. Wu, Martensitic Transformation of Grain-Size Mixed Ti<sub>51</sub>Ni<sub>49</sub> Melt-Spun Ribbons, *J. Alloys Compd.*, 2006, **424**, p 171–175
11. B. Strnadl, S. Ohashi, H. Ohtsuka, S. Miyazaki, and T. Ishihara, Effect of Mechanical Cycling on the Pseudoelasticity Characteristics of Ti-Ni and Ti-Ni-Cu Alloys, *Mater. Sci. Eng., A*, 1995, **203**, p 187–196
12. L. Jordan, M. Masse, J.Y. Collier, and G. Bouquet, Effects of Thermal and Thermomechanical Cycling on the Phase-Transformations in NiTi and Ni-Ti-Co Shape-Memory Alloys, *J. Alloys Compd.*, 1994, **211**, p 204–207
13. Y. Liu and P.G. McCormick, Factors Influencing the Development of Two-Way Shape Memory in NiTi, *Acta Metall. Mater.*, 1990, **38**, p 1321–1326
14. C.P. Frick, A.M. Ortega, J. Tyber, A.E.M. Maksound, H.J. Maier, and Y.N. Liu, Thermal Processing of Polycrystalline NiTi Shape Memory Alloys, *Mater. Sci. Eng., A*, 2005, **405**, p 34–49
15. M. Carroll, C. Somsen, and G. Eggeler, Multiple-Step Martensitic Transformations in Ni-Rich NiTi Shape Memory Alloys, *Scripta Mater.*, 2004, **50**, p 187–192
16. D. Favier, Y. Liu, and P.G. McCormick, Three Stage Transformation Behaviour in Aged NiTi, *Scripta Metall. Mater.*, 1993, **28**, p 669–672
17. H.C. Lin, S.K. Wu, T.S. Chou, and H.P. Kao, The Effects of Cold Rolling on the Martensitic Transformation of an Equiatomic TiNi Alloy, *Acta Metall. Mater.*, 1991, **39**, p 2069–2080
18. K. Wada and Y. Liu, Thermomechanical Training and the Shape Recovery Characteristics of NiTi Alloys, *Mater. Sci. Eng., A*, 2008, **481–482**, p 166–169
19. Y. Liu and P.G. McCormick, Martensitic Transformations, *Proc. ICOMAT-92*, Monterrey Institute of Advanced Studies, 1993, p 923